

Optimal Transmitter Placement in Realistic Urban Environments

Lukas Taus, Richard Tsai, and Jeffrey G. Andrews, *Fellow, IEEE*

Abstract—In a wireless network, the spatial location of the transmitters has a large impact on the achievable rate at each user location. The optimal placement of – for example – cellular base stations is a difficult non-convex problem, and is usually addressed with simplified propagation models and simplified heuristics that may account for specifics such as the site topology, building locations, and user density. We propose a mathematically rigorous framework for optimal transmitter placement that explicitly integrates detailed site-specific maps, spatial material properties, and realistic signal attenuation. We introduce a novel aggregated network quality functional which captures the essential trade-off between maximizing network coverage and minimizing cost, and establish the problem’s submodularity under certain practical conditions. To solve the resulting resource-constrained optimization problem for sparse, discrete transmitter configurations, we propose the Interference-Aware Submodular Placement Algorithm (IA-SPA) and prove theoretical performance guarantees on its gap from optimality. IA-SPA is general and can incorporate existing BS locations and prohibited areas (e.g. a lake), making it useful for either clean-slate or incremental deployments. We show the utility of our approach using a ray tracing-based simulation framework applied to 3D maps of San Francisco and Florence, where we compare to known base station deployments by AT&T, T-Mobile and Iliad. We demonstrate that our proposed placement strategy achieves significant increases in mean data rate (about 2x) and edge rate (2–8x) compared to existing tower deployments, using the same number of transmitters.

Index Terms—Base station placement, Site-Specific Optimization, Combinatorial Optimization, Ray Tracing, Digital Twins.

I. INTRODUCTION

In the 6G era, cellular networks will continue to slowly densify and support new spectral bands, while also becoming more amenable to data-driven optimization. Given strong constraints on network cost and energy consumption [1], the placement of each new base station should attempt to maximize the coverage and capacity enhancement it provides to the network. The rapidly improving technologies of network digital twins, based on increasingly sophisticated site-specific mapping and ray tracing, provide a promising pathway to improved network deployment and configuration [2], [3]. For these emerging tools to be able to enable significant increases

in cell edge rate and median rate through improved network deployment, they need to be harnessed by well-designed, flexible and principled optimization algorithms that are able to leverage their capabilities and approach global optima.

However, optimizing something as seemingly straightforward as base station (BS) placement is in fact very complicated. The optimal BS locations depend on not only the site-specific topology and signal propagation, but also on the user locations and demand probability density functions, and other constraints such as prohibited regions or respecting existing BS deployments. Furthermore, while each new BS increases signal quality in its immediate vicinity, it causes new interference to all the neighboring cells, and changes the association regions (cell boundaries). Thus, the performance of users in adjacent cells are strongly coupled to one another, which renders the globally optimal placement of transmitters non-convex and computationally intractable. The goal of the present paper is to provide a general and rigorous approach to BS placement, one that is able to ingest detailed site-specific information and propagation modeling, but is also computationally feasible. We focus on the downlink of a cellular network, but the framework is broadly applicable to the placement of any set of radiating transmitters.

A. Relation to Prior Work

Wireless transmitter placement is, to a first order, a geometry problem. Foundational results from the *art gallery problem* [4]–[6] establish bounds for covering polygonal environments, serving as a proxy for signal presence in high-frequency or aerial scenarios [7]. However, since finding optimal configurations is NP-hard [8], practical scalability requires greedy strategies [9]. Early efforts by Amaldi et al. [10] used randomized heuristics for UMTS planning, but relied on simplified propagation models and constant interference thresholds that lacked uniqueness.

In both robotics and communications, greedy algorithms are often used for managing the complexity of coverage problems. In robotics, *next-best-view* and exploration algorithms are used to optimize gain measures like unexplored volume or surface area [11]–[14]. In addition, multi-coverage objectives have been explored to make the sensor network more robust against failure [15]. However, a critical gap is the lack of detailed analysis on the role of interference. Most existing greedy frameworks optimize for simple area coverage or connectivity, but particularly in urban networks, interference plays a critical role near the cell edge in degrading the signal quality, i.e. the Signal-to-Interference plus Noise Ratio (SINR).

Physically grounded optimization is increasingly enabled by digital twins and ray-tracing frameworks like Sionna RT [16], which incorporate site-specific material properties and antenna

L. Taus and R. Tsai are with the Oden Institute for Computational Engineering and Sciences, The University of Texas at Austin, Austin, TX, USA (e-mail: ltaus@utexas.edu; ytsai@math.utexas.edu). Taus and Tsai are partially supported by NSF grant DMS-2208504, DMS-2513857, and Army Research Office Grant W911NF2320240.

J. G. Andrews is with 6G@UT in the Wireless Networking and Communications Group and the Dept. of Electrical and Computer Engineering at the University of Texas at Austin, Austin, TX, USA (e-mail: jandrews@ece.utexas.edu).

Manuscript last updated May 8, 2026.

This work has been submitted to the IEEE for possible publication. Copyright may be transferred without notice, after which this version may no longer be accessible.

orientations [2], [17]. Such high-fidelity modeling is critical in mmWave and reconfigurable intelligent surface (RIS) networks [18]–[21]. Methods that utilize expensive gradient based searches have been explored to optimize transmitter locations [22]. However, these methods are myopic and require a-priori knowledge of the required number of transmitters. Our method scales by approximating interference through the physical overlap of ray-traced areas, enabling a high-fidelity optimization loop at a fraction of the computational cost.

Furthermore, these methods optimize for SINR, a non-convex problem where the optimal solution is not necessarily unique [23]–[27], leaving gradient descent susceptible to sub-optimal local optima. Unlike these paradigms, which require the number of base stations to be fixed a priori, our approach dynamically determines a near-minimal site count using 3D ray-tracing for realistic geometric shadowing. By employing a submodular greedy strategy, we eliminate gradient dependency and provide formal theoretical guarantees on network quality relative to the global optimum.

To bypass the computational cost of high-fidelity simulation, various acceleration techniques have been proposed, ranging from generative AI [28], [29] and neural surrogates [30] to DRL-based placement for aerial and RIS-assisted networks [31]–[33]. Other strategies employ Bayesian optimization [34], genetic algorithms [35], or multi-armed bandits [36] for transmission and site design. Additionally, terrain-aware frameworks utilize radio tomographic imaging [37]–[39] or global connectivity maps [40], [41] to optimize real-time node movement in site-specific channels.

The contribution of this paper lies in combining submodular greedy optimization with high-fidelity ray-tracing. Unlike iterative parameter tuning [42] or DRL-based deployment under EMF and coordination constraints [43], [44], our framework addresses the fundamental challenge of initial site selection. By approximating interference through the physical overlap of ray-traced coverage areas, our method provides a higher-fidelity optimization loop at a lower computational cost. As we will demonstrate, this approach scales efficiently to large numbers of receivers, yielding outstanding performance against existing deployments and benchmarks while maintaining formal theoretical guarantees.

B. Contributions

In this work, we formulate the transmitter placement problem in a manner that explicitly incorporates spatial material properties and signal attenuation effects. By introducing an aggregated network quality functional $\mathcal{S}(c)$, we capture the trade-off between network coverage and resource expenditure in a mathematically general form.

We then develop the Interference-Aware Submodular Placement Algorithm (IA-SPA), which is based on a greedy algorithm and constructs sparse, discrete tower configurations. This framework connects ideas from convex analysis, sparse optimization, and geometric signal propagation, and can be applied across domains such as telecommunications, sensor deployment, and surveillance network design. The following points highlight the core innovations of this work.

Novel Optimization Framework: We propose a rigorous mathematical framework for optimal transmitter placement that integrates physical signal propagation and spatial material properties directly from high-fidelity simulations. To address resource-constrained placement, we developed an algorithm (IA-SPA) for sparse tower configurations that offers theoretical performance guarantees.

Network Quality Functional: We introduce a novel aggregated network quality functional, $\mathcal{S}(T)$, designed to capture the trade-off between coverage, cost, and interference while maintaining sub-modularity under practical conditions. Unlike traditional area-coverage models, our framework explicitly accounts for signal degradation and interference in multi-transmitter environments.

Realistic Validation: The approach is validated using the Sionna RT ray-tracing framework applied to realistic 3D models of San Francisco and Florence, demonstrating significant throughput improvements over existing deployments by AT&T and T-Mobile in SF, and Iliad in Florence. For example, IA-SPA achieves mean throughput gains of up to 70% in dense urban scenarios and edge-rate improvements exceeding 88%, while simultaneously keeping interference low.

Constrained and Ongoing Deployments: The framework is inherently general, allowing for the optimal augmentation of existing infrastructure. Given a set of pre-deployed transmitters, the algorithm identifies new locations that provide the maximum marginal utility at minimal cost, effectively filling coverage gaps in mature networks. Our method can also handle complex spatial constraints and exclusionary zones, such as lakes or historic sites.

C. Notation and Organization

Throughout this paper, we use the following mathematical notation:

- $\Omega \subseteq \mathbb{R}^n$: A compact set representing the physical environment.
- $x, y \in \Omega$: Locations within the domain where y typically denotes a receiver position and x a transmitter position.
- $\mu(x)$: Material parameters characterizing local signal propagation (e.g., absorption, reflection).
- $P(y, x)$: The propagation function representing signal power (or SNR) received at y from a source at x .
- $T = \{t_1, \dots, t_n\}$: A discrete set of transmitter locations.
- $\mathcal{P}_{\text{SUM}}(y, T)$ & $\mathcal{P}_{\text{MAX}}(y, T)$: The cumulative network quality or power at location y given the transmitter set T .
- $f(y)$: A normalized spatial density function. This function serves as a weighting mechanism to steer the optimization toward high-priority regions. By adjusting the local magnitude of $f(y)$, the framework can accommodate heterogeneous service requirements.
- $w(\kappa)$: A weight function representing the marginal utility of network quality κ .
- $\bar{W}(x) = \int_0^x w(\kappa) d\kappa$: The anti-derivative of w .
- $\mathcal{S}(T)$: The aggregated network quality functional used as the primary optimization objective.

Organization: Section II establishes the system model, detailing the propagation environment, signal aggregation met-

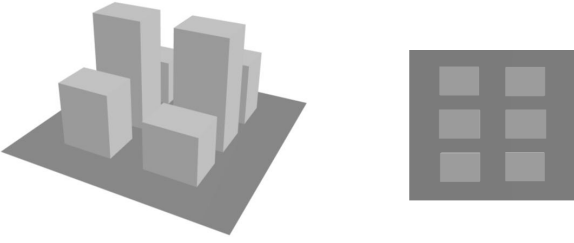


Fig. 1. A simple urban environment used as a toy example to illustrate concepts. The left image shows the 3D map and the right image shows the same environment from a top down view.

rics, and the formal optimization problem. Section III introduces the proposed IA-SPA framework, alongside an analysis of its theoretical performance guarantees and computational complexity. Section IV presents a comprehensive numerical evaluation using high-fidelity 3D ray tracing in San Francisco and Florence, exploring diverse deployment scenarios including exclusionary zones and incremental network expansion. Finally, Section V discusses the broader implications of our findings and provides concluding remarks.

II. SYSTEM MODEL AND PROBLEM FORMULATION

Let $\Omega \subseteq \mathbb{R}^n$ be a compact set representing the environment. We assume the environment is composed of regions with different material properties, which determine how a signal propagates through space. Each point $x \in \Omega$ is associated with material parameters $\mu(x)$ that characterizes the local propagation behavior of the signal, such as its ability to **absorb**, **refract**, or **reflect** incoming signals.

To illustrate the concepts underlying our mathematical formulations and methods, we will use the simple environment shown in Fig. 1. In section IV we will present results for a realistic environment such as San Francisco and Florence (see Fig. 5).

A. Propagation Model

We define the propagation function $P(y, x)$, which represents the signal power received at location $y \in \Omega$ when the signal originates from a source at location $x \in \Omega$ and propagates through the environment Ω according to the material-dependent properties $\mu(x)$.

In modern wireless network design, $P(y, x)$ serves as the physical foundation for determining the local data rate. While classical models often rely on binary Line-of-Sight (LoS) visibility to simplify propagation into regions of total coverage or total occlusion [7], such abstractions are increasingly replaced by higher-fidelity methods to capture the "cliff effects" of high-frequency bands.

Depending on the required balance between physical realism and computational cost, $P(y, x)$ can be derived from several modeling paradigms:

- **Ray-tracing methods**, which simulate the reflection and refraction of rays as they interact with material boundaries.
- **Line-of-sight (LOS)-based visibility functions**, which simplify propagation to binary occlusion. [7]
- **Wave-based models**, which capture scattering and multi-path effects.

In the following, $P(y, x)$ is considered to be the Signal-to-Noise Ratio (SNR) at location y from a transmitter at x . Without loss of generality, we assume a normalized noise power of $\sigma^2 = 1$, such that $P(y, x)$ also corresponds to the received signal power at y . Fig. 2 illustrates $P(y, x)$, computed for the environment in Fig. 1 using Sionna. Each panel shows the propagation for a different transmitter location x (red marker). The resulting color map at y represents the data rate, demonstrating how environmental geometry and material properties transform a simple source into a complex coverage field.

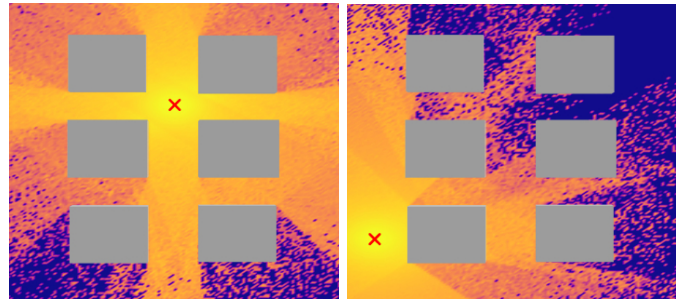


Fig. 2. $P(y, x)$ for an urban environment. The red marker indicates the transmitter position x and the colors represent the data rate at each location y which corresponds to the values of $P(y, x)$.

We present a formulation and algorithm that does not rely on a specific model for $P(y, x)$, any physically or empirically motivated signal propagation model can be substituted without affecting the structure or validity of the algorithm.

B. Network Quality and SINR

To describe the interaction of multiple transmitters in the set $T = \{t_1, t_2, \dots, t_n\}$ in the environment, we use the function $\mathcal{P}(y, T)$ which describes the cumulative power at location $y \in \Omega$. In practice this is done by

$$\text{SINR}(y, T) = \frac{\max_{t \in T} P(y, t)}{\sum_{t \in T} P(y, t) - \max_{t \in T} P(y, t) + \sigma^2} \quad (1)$$

This formula assumes that at any location at the environment $y \in \Omega$, a user will connect to the transmitter with the best available signal and all other towers interfere with the communication. While this ratio accurately reflects the local throughput, it presents significant challenges for global optimization. As discussed in [23]–[27], the fractional nature of the SINR leads to a non-convex optimization landscape with many local optima, complicating the search for an optimal deployment configuration. To facilitate a more robust optimization framework with theoretical guarantees, we utilize the following aggregated proxy measures.

Definition II.1 (Aggregated Network Quality). Given functions $P(y, x)$ and a transmitter set $T = \{t_1, \dots, t_n\}$, we define the following cumulative measures to represent the total signal quality at a location x :

- 1) **Maximum Signal Selection** (\mathcal{P}_{MAX}):

$$\mathcal{P}_{\text{MAX}}(y, T) = \max_{x \in T} P(y, x) \quad (2)$$

This formulation is the classical choice for systems where all transmitters operate on the same frequency. In this scenario, the user associates only with the strongest available signal, while other signals are treated as interference rather than contributing to the useful signal power.

- 2) **Aggregate Signal Power** (\mathcal{P}_{SUM}):

$$\mathcal{P}_{\text{SUM}}(y, T) = \sum_{x \in T} P(y, x) \quad (3)$$

This measure defines an idealized upper bound by treating all detectable transmissions from the set T as constructive signal components. It represents the total available energy at receiver y before accounting for interference.

In Fig. 3 we show the aggregated network quality function $\mathcal{P}_{\text{SUM}}(y, T)$ on the simple environment shown in Fig. 1. In the shown example $T = \{t_1, \dots, t_n\}$ where the cyan markers show the positions of t_i . The colors of the figure correspond to the value of $\mathcal{P}_{\text{SUM}}(y, T)$.

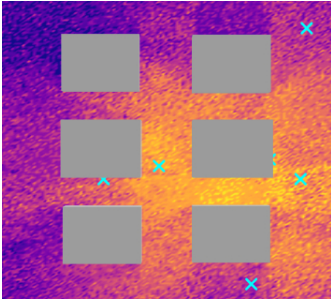


Fig. 3. Example of the aggregated network quality function $\mathcal{P}_{\text{SUM}}(y, T)$. The cyan markers indicate the position of the transmitters and the colors indicate the aggregated network quality in the environment.

C. Accommodating Deployment Constraints

In practical network planning, transmitter placement is often governed by environmental, regulatory, or infrastructural constraints that render large portions of the domain Ω unsuitable for deployment. Our framework accommodates these restrictions by defining a set of candidate locations $\mathcal{X} \subset \Omega$. Locations $x \notin \mathcal{X}$ (e.g., bodies of water, or protected parks) are excluded from consideration by enforcing:

$$P(y, x) \equiv 0 \quad \forall y \in \Omega, \text{ if } x \notin \mathcal{X}. \quad (4)$$

This effectively restricts the search space of the optimization algorithm to a feasible discrete or continuous subset without requiring a change in the underlying objective functional.

Furthermore, the algorithm naturally supports *incremental deployment* through a non-empty initial condition. Let T_{fixed} represent a set of pre-existing transmitters whose locations are permanent. The optimization problem then becomes:

$$\max_{T \subset \mathcal{X}, |T| \leq k} \mathcal{S}(T \cup T_{\text{fixed}}). \quad (5)$$

Because the aggregated network quality functional \mathcal{S} is sub-modular, the IA-SPA remains highly effective for selecting the remaining k transmitters. This approach allows network operators to optimize new infrastructure placement while accounting for the coverage and interference footprints of the current network, or to mandate the use of specific high-priority sites before selecting auxiliary locations.

D. Optimization Problem Formulation

Our general goal is to find the optimal transmitter configuration to maximize the average throughput and coverage in the environment Ω .

In practice, the demand of wireless connectivity is rarely uniform across the service domain Ω . Urban environments typically exhibit heterogeneous traffic patterns, where high-occupancy areas (such as public squares, transit hubs, or office complexes) require significantly higher resource allocation than parks or industrial zones. To incorporate this into our optimization framework we define the spatial priority density function $f: \Omega \rightarrow \mathbb{R}_+$.

This density function f serves as a local weighting mechanism that scales the utility contribution of each point $y \in \Omega$ according to the expected required resources in the area. From a probabilistic perspective, f can be interpreted as the probability density function of user locations.

Furthermore, the perceived utility of increased network quality behaves non-linearly. In regions where connectivity is already high, further improvements yield diminishing returns. To capture this characteristic, we introduce a weight function $w(\kappa)$ that assigns a relative value to different levels of the aggregated network quality κ . Specifically, $w(\kappa)$ represents the marginal increase in utility gained by improving the network quality at a current state κ . We assume that $w \geq 0$ and that transmitters are chosen from a set of candidates $T \subseteq \mathcal{X} \subseteq \Omega$ with $|\mathcal{X}| < \infty$. This ensures that the total possible utility in the environment remains bounded since

$$\mathcal{P}(y, T) \leq \mathcal{P}(y, \mathcal{X}) \leq \sup_{y \in \Omega} \mathcal{P}(y, \mathcal{X}) =: M < \infty, \quad (6)$$

and therefore

$$\bar{W}(x) = \int_0^x w(\kappa) d\kappa \leq \int_0^M w(\kappa) d\kappa < \infty, \quad (7)$$

for all $x = \mathcal{P}(y, T)$ for some $y \in \Omega$ and some $T \subseteq \mathcal{X}$.

Remark II.2. We would like to point out that these assumptions on \bar{W} are not very restrictive and allow for a wide range of utility functions including

$$\bar{W}(x) = \log(1 + x) \quad \text{and} \quad \bar{W}(x) = \frac{x}{x + c}. \quad (8)$$

Taking all these considerations into account, we can formulate a function which measures the value of a set of transmitters T using the function

$$S(T) = \int_0^M w(\kappa) \int_{\Omega} \mathbb{1}_{\{\mathcal{P}(y,T) > \kappa\}} f(y) dy d\kappa. \quad (9)$$

It is easy to see that S is monotone

$$T_1 \subseteq T_2 \implies S(T_1) \leq S(T_2). \quad (10)$$

In practice we usually want to achieve a given value using minimal number of transmitters to minimize cost. This yields the constraint optimization problem

$$\min_T |T| \quad \text{s.t. } S(T) \geq \beta, \quad (11)$$

where $|T|$ denotes the cardinality of the transmitter set T . Alternatively we might also have access to a limited amount of resources and we want to achieve the optimal value within those resources which leads to the related constraint optimization problem

$$\max_T S(T) \quad \text{s.t. } |T| \leq \beta. \quad (12)$$

Theorem II.3. Let $X \sim f$ and $\bar{W}(x) = \int_0^x w(\kappa) d\kappa$. Then

$$S(T) = \mathbb{E}_X[\bar{W}(\mathcal{P}(X, T))]. \quad (13)$$

Proof of Theorem II.3. Let X be a random variable with density function f in Ω , then

$$\int_{\Omega} \mathbb{1}_{\{\mathcal{P}(x,T) > \kappa\}} f(x) dx = \mathbb{P}[\mathcal{P}(X, T) > \kappa]. \quad (14)$$

Define the random variable $Y = \mathcal{P}(x, T)$, then

$$\mathbb{P}[\mathcal{P}(X, T) > \kappa] = 1 - F_Y(\kappa), \quad (15)$$

where F_Y is the cdf of the random variable Y . This shows

$$S(T) = \int_0^M w(\kappa)(1 - F_Y(\kappa)) d\kappa. \quad (16)$$

Using Riemann-Stieltjes integrals know

$$\mathbb{E}[\bar{W}(Y)] = \int \bar{W}(x) dF_Y(x). \quad (17)$$

Since $w \geq 0$, \bar{W} is monotone increasing. Thus we can apply integration by parts to the above expression to get

$$\int \bar{W}(x) dF_Y(x) = [\bar{W}(x)F_Y(x)]_0^M - \int F_Y(x) d\bar{W}(x). \quad (18)$$

Since F_Y is a cdf, we know

$$\lim_{x \rightarrow \infty} F_Y(x) = 1 \quad \text{and} \quad \lim_{x \rightarrow 0} F_Y(x) = 0. \quad (19)$$

Further by definition of \bar{W} we know

$$\lim_{x \rightarrow 0} \bar{W}(x) = \lim_{x \rightarrow 0} \int_0^x w(\kappa) d\kappa = 0 \quad (20)$$

and we assume that

$$\lim_{x \rightarrow M} \bar{W}(x) = \int_0^M w(\kappa) d\kappa < \infty. \quad (21)$$

This yields

$$[\bar{W}(x)F_Y(x)]_0^M = \int_0^M w(\kappa) d\kappa. \quad (22)$$

Since $\bar{W}(x) = \int_0^x w(\kappa) d\kappa$ it is obviously differentiable and its derivative is w . Thus

$$\int F_Y(x) d\bar{W}(x) = \int F_Y(x) w(x) dx. \quad (23)$$

By plugging these results into the formula above, we see that

$$\int \bar{W}(x) dF_Y(x) = \int (1 - F_Y(\kappa)) w(\kappa) d\kappa. \quad (24)$$

This shows

$$S(T) = \int_0^M w(\kappa)(1 - F_Y(\kappa)) d\kappa = \mathbb{E}[\bar{W}(\mathcal{P}(X, T))]. \quad (25)$$

□

Note that both problem statements described in equations (11) and (12) yield a convex optimization problem if $S(T)$ is concave. In this context concavity of S is defined as

$$S(A \cup \{t\}) - S(A) \geq S(B \cup \{t\}) - S(B). \quad (26)$$

for any $A \subseteq B \subset \Omega$ and any $t \in \Omega \setminus B$.

Theorem II.3 allows us to analyze the concavity of S . We know that the expectation is a linear function and therefore preserves concavity. Further since $w(\kappa) \geq 0$ and $\bar{W}(x) = \int_0^x w(\kappa) d\kappa$, we know that \bar{W} is non-decreasing.

Theorem II.4. If \bar{W} is concave and for any $y \in \Omega$ $T \mapsto \mathcal{P}(y, T)$ is convex, then $S(T)$ is concave, and therefore the problems described by equations (11) and (12) are convex.

Theorem II.4 shows that as long as we pick the weights w such that its anti-derivative \bar{W} is concave, the resulting constraint optimization problems are convex for both $\mathcal{P} = \mathcal{P}_{\text{MAX}}$ and $\mathcal{P} = \mathcal{P}_{\text{SUM}}$ and therefore admit globally optimal solutions. This can be interpreted as a concave \bar{W} leading to diminishing returns.

Remark II.5. Since \bar{W} is assumed to be concave, it assigns higher value to improvements at small throughput regions. Therefore algorithm 1 will prioritize regions that are further away from existing transmitters and therefore implicitly reducing interference.

The optimization problems introduced above can be approached in multiple ways, depending on whether we seek a discrete or continuous representation of the transmitter field. In the following, we first present a constructive IA-SPA that incrementally selects optimal transmitter locations when the solution is assumed to be a sum of Dirac measures. This algorithm directly targets the discrete, resource-constrained formulation and provides explicit performance guarantees.

III. PROPOSED FRAMEWORK AND ALGORITHM

In this section we describe the IA-SPA to approximate the optimal transmitter set T . This is done by computing the transmitter locations sequentially by computing which location

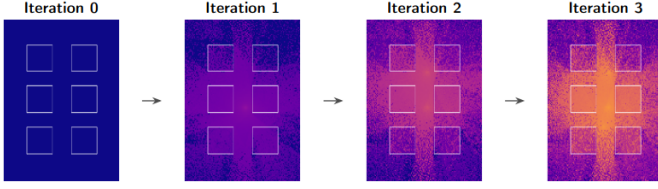


Fig. 4. Achieved coverage for the first 3 iteration of Algorithm 1.

improves the utility of the existing transmitter the most. To measure this we define the gain function by

$$\mathcal{G}(x|T) = \mathcal{S}(T \cup \{x\}) - \mathcal{S}(T). \quad (27)$$

This measures how much utility we gain by placing an additional transmitter at the location $x \in \Omega$. Performing this iteratively yields the IA-SPA

Algorithm 1 IA-SPA

$T = []$ or $T = T_{\text{fixed}}$

while not Terminated **do**

 Calculate $\mathcal{G}(x|T)$ for every $x \in \Omega$

 Let $\Omega_\epsilon = \{y \in \Omega \mid \mathcal{G}(y|T) \geq (1 - \epsilon) \max_{z \in \Omega} \mathcal{G}(z|T)\}$

 Choose $x^* \in \Omega_\epsilon$ uniformly at random

$T.append(x^*)$

end while

Note that by changing the termination criteria, Algorithm 1 is capable of solving both problems described by equation (11) and (12). For equation (11), we can pick the termination criteria

$$S(T) \geq M \quad (28)$$

and for equation (12) the algorithm is terminated after M iterations, satisfying $|T| = M$.

For the current set of transmitters T , the gain function $G(x, T)$ is computed. The feasible region $\Omega_\epsilon = \{y \in \Omega \mid \mathcal{G}(y|T) \geq (1 - \epsilon) \max_{z \in \Omega} \mathcal{G}(z|T)\}$ is then determined and the next transmitter location is chosen at random from this set and the transmitter configuration is updated. These steps are repeated until the desired coverage is achieved or the resource limit is reached. Fig. 4 shows the resulting coverage (communication speed) that has been achieved across the iterations of Algorithm 1.

A. Theoretical Guarantee on Network Quality

Proposition III.1. If \bar{W} is concave, then

$$\forall x \in \Omega: T_1 \subseteq T_2 \implies G(x|T_1) \geq G(x|T_2) \quad (29)$$

This expresses the principle of diminishing returns. As more transmitters are added, the marginal benefit of an additional one decreases when \bar{W} is concave.

This proposition allows us to compute a guaranteed lower bound for the resulting coverage function when using the IA-SPA

Theorem III.2. Let T_k^* be a solution of

$$\arg \max_T \mathcal{S}(T) \quad \text{s.t. } |T| = k \quad (30)$$

and let T_n be the sequence of n transmitters generated by the IA-SPA with parameter ϵ . Then if \bar{W} is concave

$$\left(1 - e^{-\frac{n(1-\epsilon)}{k}}\right) \mathcal{S}(T_k^*) \leq \mathcal{S}(T_n). \quad (31)$$

Proof of Theorem III.2. Since $T_k^* \subseteq T_k^* \cup T_n$, we get by monotonicity of S that

$$\mathcal{S}(T_k^*) \leq \mathcal{S}(T_k^* \cup T_n). \quad (32)$$

We denote the entries of $T_k^* = \{y_1^*, \dots, y_k^*\}$ in any order. Then

$$\mathcal{S}(T_k^* \cup T_n) = \mathcal{S}(T_n) + \sum_{j=1}^k \mathcal{S}(T_n \cup \{y_1^*, \dots, y_j^*\}) - \mathcal{S}(T_n \cup \{y_1^*, \dots, y_{j-1}^*\}), \quad (33)$$

and by definition of \mathcal{G} , this is

$$\mathcal{S}(T_k^* \cup T_n) = \mathcal{S}(T_n) + \sum_{j=1}^k \mathcal{G}(y_j^* | T_n \cup \{y_1^*, \dots, y_{j-1}^*\}). \quad (34)$$

By concavity of S , since $T_n \subseteq T_n \cup \{y_1^*, \dots, y_{j-1}^*\}$ for any j , this shows

$$\mathcal{S}(T_k^*) \leq \mathcal{S}(T_n) + \sum_{j=1}^k \mathcal{G}(y_j^* | T_n). \quad (35)$$

We know that T_n contains the points chosen by Algorithm 1 and that the algorithm chooses points such that

$$\mathcal{G}(x_{n+1} | T_n) \geq (1 - \epsilon) \sup_{x \in \Omega} \mathcal{G}(x | T_n). \quad (36)$$

Thus for any $y \in \Omega$ (specifically also for y_j^*)

$$\mathcal{G}(y | T_n) \leq \sup_{x \in \Omega} \mathcal{G}(x | T_n) \leq \frac{1}{1 - \epsilon} \mathcal{G}(x_{n+1} | T_n). \quad (37)$$

This shows

$$\mathcal{S}(T_k^*) \leq \mathcal{S}(T_n) + \frac{k}{1 - \epsilon} \mathcal{G}(x_{n+1} | T_n), \quad (38)$$

and by plugging in the definition of \mathcal{G} , we get

$$\mathcal{S}(T_k^*) - \mathcal{S}(T_n) \leq \frac{k}{1 - \epsilon} (\mathcal{S}(T_{n+1}) - \mathcal{S}(T_n)). \quad (39)$$

Define the sequence

$$\Delta_n = \mathcal{S}(T_k^*) - \mathcal{S}(T_n), \quad (40)$$

then the inequality above shows

$$\Delta_n \leq \frac{k}{1 - \epsilon} (\mathcal{S}(T_{n+1}) - \mathcal{S}(T_n)) = \frac{k}{1 - \epsilon} (\Delta_n - \Delta_{n+1}). \quad (41)$$

This shows

$$\left(1 - \frac{1 - \epsilon}{k}\right) \Delta_n \geq \Delta_{n+1}. \quad (42)$$

Since $\frac{1 - \epsilon}{k} \in (0, 1)$, we can further estimate by using

$$1 - x \leq e^{-x} \quad \text{for } x \in (0, 1). \quad (43)$$

TABLE I
RESULTS COMPARISON USING \mathcal{P}_{MAX} COMPARED TO THE AVERAGE OF 10
RANDOM LOCATIONS

Throughput [MBps]	Random	IA-SPA	Change
Mean Rate	10.42	36.10	↑ 246.41%
Edge (5% pct.)	1.48	10.36	↑ 598.96%
Interference [nW]	Reference	IA-SPA	Change
Mean Interf.	0.46	2.19	↑ 377.52%

Thus

$$\Delta_{n+1} \leq e^{-\frac{1-\epsilon}{k}} \Delta_n. \quad (44)$$

Note that since $S(\emptyset) = 0$, $\Delta_0 = S(T_k^*) - S(\emptyset) = S(T_k^*)$. Thus we can solve the recursion which yields

$$\Delta_n \leq e^{-\frac{n(1-\epsilon)}{k}} S(T_k^*). \quad (45)$$

By plugging in the definition of Δ_n , this is

$$S(T_k^*) - S(T_n) \leq e^{-\frac{n(1-\epsilon)}{k}} S(T_k^*), \quad (46)$$

which shows

$$\left(1 - e^{-\frac{n(1-\epsilon)}{k}}\right) S(T_k^*) \leq S(T_n). \quad (47)$$

□

This provides a guaranteed coverage ratio between the results of the IA-SPA and the theoretical optimal configurations. Although the theoretical constant is conservative, it parallels the classical submodular bound which has been observed to perform much better in practice.

Remark III.3. For $n = k$ and $\epsilon = 0$, the theorem states that we achieve at least 63% of the optimal coverage value.

While Theorem III.2 provides a conservative lower bound of 63% of the optimal value, the algorithm consistently outperforms this guarantee by a wide margin in practice. To quantify this empirically, we compare IA-SPA against a random placement baseline: candidate sites are drawn uniformly at random from the same discrete set \mathcal{X} that the algorithm selects from, and 9 towers are placed in both cases to match the configuration used in the AT&T scenario of Section IV. Because random placement is stochastic, we average the performance metrics over 10 independent draws of 9 towers each. As shown in Table I, IA-SPA achieves a 246% improvement in mean throughput and a 599% improvement in edge rate (5th percentile) over this random baseline, while the random baseline actually *lowers* mean interference relative to a single transmitter due to the accidental spread of sites across the domain. These results confirm that the theoretical bound of Theorem III.2 is highly conservative, and that the greedy submodular strategy reliably identifies a near-optimal spatial configuration rather than merely outperforming worst-case guarantees.

B. Computational Complexity

Let \mathcal{X} be the set of candidate transmitter locations and Ω_δ be the discretized spatial grid (receiver points). We assume the propagation fields $P(y, x)$ are pre-computed for all $x \in \mathcal{X}$ and $y \in \Omega_\delta$.

1) Cost of Functional Evaluation $\mathcal{S}(T)$

To evaluate $\mathcal{S}(T)$ at a set T , we must:

- Aggregate by applying \mathcal{P} : $O(|T| \cdot |\Omega_\delta|)$.
- Apply the weight function \bar{W} : $O(|\Omega_\delta|)$.
- Integrate of Ω_δ : $O(|\Omega_\delta|)$

Thus, a single evaluation of $\mathcal{S}(T)$ is $O(|T| \cdot |\Omega_\delta|)$.

2) Cost per Iteration

In each iteration, the algorithm evaluates the marginal gain $\mathcal{G}(y | T) = \mathcal{S}(T \cup \{x\}) - \mathcal{S}(T)$ for every $x \in \mathcal{X}$. Since $\mathcal{S}(T)$ is already known from the previous step, we only compute $\mathcal{S}(T \cup \{x\})$.

- Cost per candidate: $O((|T| + 1) \cdot |\Omega_\delta|)$
- Total for $|\mathcal{X}|$ candidates: $O(|\mathcal{X}| \cdot |T| \cdot |\Omega_\delta|)$

3) Total Complexity

To select n transmitters, we sum

$$\sum_{i=1}^n O(|\mathcal{X}| \cdot i \cdot |\Omega_\delta|) = O(|\mathcal{X}| \cdot n^2 \cdot |\Omega_\delta|) \quad (48)$$

The computational complexity of IA-SPA is dominated by the evaluation of the aggregated quality functional over the discretized domain Ω_δ . Given $|\mathcal{X}|$ candidate sites and n target transmitters, the algorithm scales as $O(|\mathcal{X}|n^2|\Omega_\delta|)$. While the quadratic dependence on n is standard for greedy submodular maximization, the pre-computation of the ray-tracing fields $P(y, x)$ allows the iterative selection process to remain highly efficient even for dense urban environments.

IV. NUMERICAL RESULTS

In this section, we evaluate the performance of the proposed IA-SPA for optimal tower placement. All experiments were conducted using the `sienna` Python package, which provides a differentiable simulation framework for wireless communication systems, including ray tracing-based channel modeling.

A. Simulation Setup

The simulation environment was constructed using two distinct 3D models included in the `sienna` library: a dense urban model of San Francisco and Florence (see Fig. 5). These environments provide realistic building geometries and material properties, enabling physically accurate propagation and reflection modeling via ray tracing. We restricted feasible transmitter locations to a height of 20 meters above the terrain. The system parameters were set to a carrier frequency of 1.8 GHz, a transmit power of 40 dBm (10 W), and a bandwidth of 10 MHz.

To ensure a realistic baseline for comparison, we utilized ground-truth transmitter data from two primary sources. For the San Francisco scenarios, we leveraged coordinates from the City and County of San Francisco's open data portal [45]. To further validate the framework across different carrier

deployments (Iliad, TIM, and Vodafone), we integrated cell tower data from the OpenCellID database [46]. This allowed us to initialize the environment with the exact locations of currently operational infrastructure.

The tower coordinates were mapped onto the `sienna` environments, and the ray tracing engine was used to compute the received power field. To map these physical signal levels to network performance, we calculate the achievable data rate at each location x using the Shannon capacity formula.

$$C(x) = B \log_2 \left(1 + \frac{\text{SINR}(x)}{\Gamma} \right), \quad (49)$$

where B is the 10 MHz bandwidth, the Gap $\Gamma = 2$ (3 dB), and the SINR is derived from the aggregated quality measures \mathcal{P}_{MAX} and \mathcal{P}_{SUM} defined in Section II.

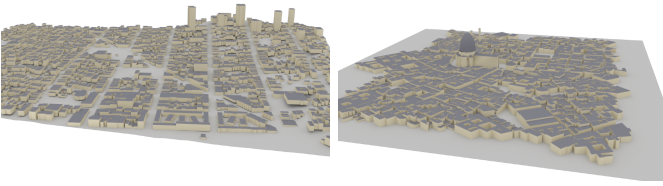


Fig. 5. 3D maps of San Francisco (left) and Florence (right) included in Sienna.

B. Performance Metrics

Using the computed field $P(y, x)$, we applied the proposed IA-SPA to determine a set of optimal tower locations. We compared the performance of using \mathcal{P}_{MAX} and \mathcal{P}_{SUM} as accumulation functions. The algorithm iteratively selects the sites that yield the greatest incremental improvement in network performance.

The results of algorithm 1 are then compared to the transmitter locations extracted from the data set. We look at the throughput and interference averaged over heights 1.5m, 5m, 10m, and 20m for a comprehensive comparison.

C. San Francisco using \mathcal{P}_{MAX}

The IA-SPA optimization framework yields significant performance gains over existing infrastructure, nearly doubling mean throughput in established carrier scenarios. As detailed in Table II, the mean data rate increased by 70% in the AT&T scenario and by over 215% in the T-Mobile scenario. Even more striking is the improvement at the network edge (5th percentile), which saw increases of 88% and 758%, respectively. Remarkably, these capacity gains were achieved while simultaneously reducing network interference slightly by 2% for AT&T and a drastic 93% for T-Mobile, proving that the algorithm successfully disentangles overlapping signal footprints by exploiting site-specific 3D geometry.

Fig. 6 illustrates this spatial distribution, where IA-SPA achieves higher consistency across the simulated area. This is particularly evident in high-density urban blocks where traditional line-of-sight coverage is typically limited.

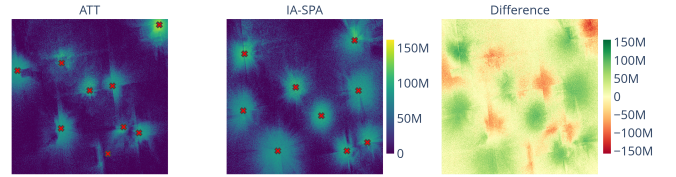


Fig. 6. Achieved throughput across San Francisco for the optimized (using \mathcal{P}_{MAX}) and existing (AT&T) transmitter locations.

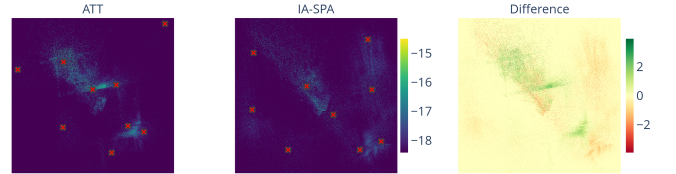


Fig. 7. Interference within the transmitter network across San Francisco for the optimized (using \mathcal{P}_{MAX}) and existing transmitter locations.

The IA-SPA framework delivers transformative capacity gains, nearly doubling mean throughput while simultaneously lowering the network interference floor. As detailed in Table II, the mean data rate increased by 70% for the AT&T scenario and over 215% for T-Mobile. These improvements are most pronounced at the network edge (5th percentile), where rates surged by 88% and 758%, respectively. Notably, these gains do not come at the cost of signal quality; interference decreased by 2% in the AT&T case and a drastic 93% in the T-Mobile case, proving that the algorithm successfully disentangles overlapping signal footprints.

D. San Francisco using \mathcal{P}_{SUM}

While the \mathcal{P}_{SUM} model provides a baseline for aggregate power, it consistently yields lower marginal gains than the \mathcal{P}_{MAX} objective. Under this power-summation model, IA-SPA still outperforms reference configurations—achieving a 43% increase in mean throughput for AT&T and 177% for T-Mobile (Table III), but the magnitude of improvement is noticeably reduced compared to \mathcal{P}_{MAX} .

Fig. 8 illustrates the spatial distribution of communication speeds obtained, and Fig. 9 the interference using \mathcal{P}_{SUM} .

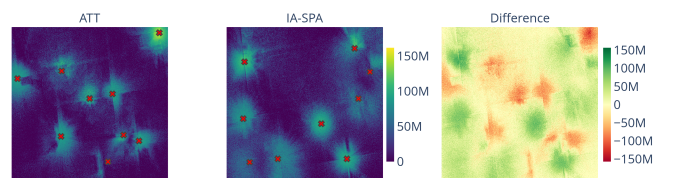


Fig. 8. Achieved throughput across San Francisco for the optimized (using \mathcal{P}_{SUM}) and existing (AT&T) transmitter locations.

TABLE II
RESULTS COMPARISON USING \mathcal{P}_{MAX}

Throughput [Mbps]	AT&T Scenario			T-Mobile Scenario		
	Reference	IA-SPA	Change	Reference	IA-SPA	Change
Mean Rate	21.18	36.1	↑ 70.4%	10.06	31.72	↑ 215.49%
Std. Deviation	26.21	28.84	↑ 10.01%	20.24	29.75	↑ 47.01%
Max Rate	146.35	116.50	↓ 20.4%	154.24	125.72	↓ 18.49%
Edge (5% pct.)	5.51	10.36	↑ 88%	1.11	9.55	↑ 758.39%
Interference [nW]	Reference	IA-SPA	Change	Reference	IA-SPA	Change
Mean Interf.	2.24	2.19	↓ 2.04%	17.54	1.11	↓ 93.70%
Std. Deviation	11.53	8.58	↓ 25.57%	216.76	5.22	↓ 97.59%
Max Interf.	495.86	473.93	↓ 4.42%	20491.9	214.04	↓ 98.96%

TABLE III
RESULTS COMPARISON USING \mathcal{P}_{SUM}

Throughput [Mbps]	AT&T Scenario			T-Mobile Scenario		
	Reference	IA-SPA	Change	Reference	IA-SPA	Change
Mean Rate	21.17	30.43	↑ 43.76%	10.06	27.92	↑ 177.62%
Std. Deviation	26.90	27.18	↑ 1.04%	20.24	27.94	↑ 38.04%
Max Rate	162.00	125.57	↓ 22.49%	154.24	125.57	↓ 18.59%
Edge (5% pct.)	3.57	4.90	↑ 37.10%	1.11	6.47	↑ 482.24%

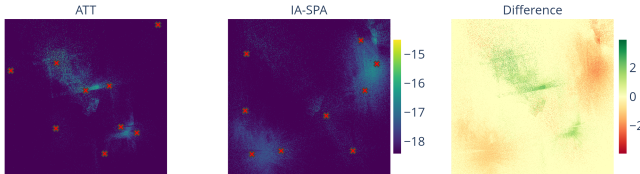


Fig. 9. Interference within the transmitter network across San Francisco for the optimized (using \mathcal{P}_{SUM}) and existing transmitter locations.

We also compare the quantitative performance measures as in the previous section in Table III.

Even under the more conservative \mathcal{P}_{SUM} model, IA-SPA consistently outperforms established carrier configurations by prioritizing a more robust distribution of signal power. In the AT&T scenario, the optimization achieved a 43% increase in mean throughput and a 37% improvement in edge performance (Table III). While these gains are less aggressive than those seen under \mathcal{P}_{MAX} , they confirm that the algorithm effectively identifies strategic transmitter sites that mitigate urban “dead zones” regardless of the power aggregation model used.

E. Florence with Exclusionary Zone

To demonstrate the flexibility of the IA-SPA algorithm in handling real-world deployment constraints, we conduct a numerical study using the Sionna *florence* map. In this scenario, we define an exclusionary zone, represented by an elliptical region surrounding the Basilica di San Lorenzo, where transmitter placement is strictly prohibited due to regulatory or historical preservation requirements. This is implemented

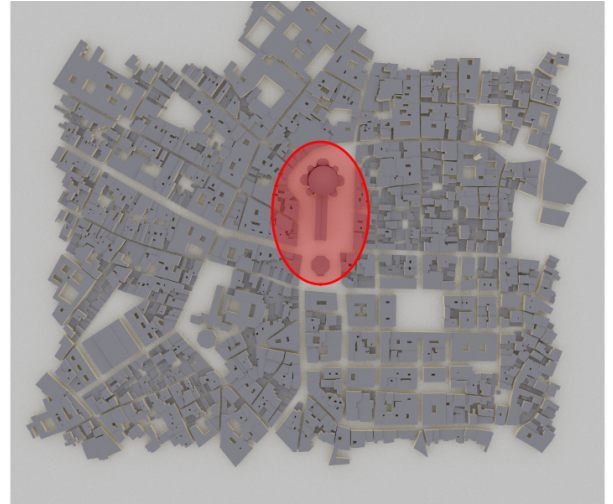


Fig. 10. Top-down view of the Florence simulation environment. The red ellipse denotes a geographically constrained exclusionary zone (centered on the Basilica di San Lorenzo) where transmitter placement is prohibited. The IA-SPA must optimize network coverage by selecting sites exclusively from the remaining feasible urban domain.

within our framework by restricting the candidate set \mathcal{X} such that $P(y, x) \equiv 0$ for all x within the red elliptical boundary. Fig. 10 provides a top-down visualization of the urban environment, highlighting the interplay between the restricted heritage site and the feasible deployment domain.

IA-SPA maintains its optimization efficacy even when deprived of the central candidate sites. In the Florence study, the algorithm achieved a substantial 55% improvement in

the edge data rate (5th percentile) compared to the Iliad baseline, despite the total prohibition of transmitters within the historical Basilica di San Lorenzo zone (Fig. 10). This robust performance proves that the framework does not merely rely on “easy” placements, but identifies non-obvious sites that maximize service for users in vulnerable, shadowed regions.

TABLE IV
PERFORMANCE COMPARISON: ILIAD BASELINE VS. IA-SPA (FLORENCE WITH EXCLUSIONARY ZONE)

Metric	Iliad Dataset	IA-SPA	Change
<i>Data Rate [Mbps]</i>			
Mean Data Rate	39.21	50.96	↑29.98%
Standard Deviation	29.38	29.28	↓0.33%
Maximum Data Rate	204.79	207.76	↑1.45%
Edge Rate (5%-tile)	7.41	11.53	↑55.62%
<i>Interference [nW]</i>			
Mean Interference	8.54	5.94	↓30.48%
Standard Deviation	18.20	6.99	↓61.61%
Maximum Interference	499.86	249.05	↓50.18%

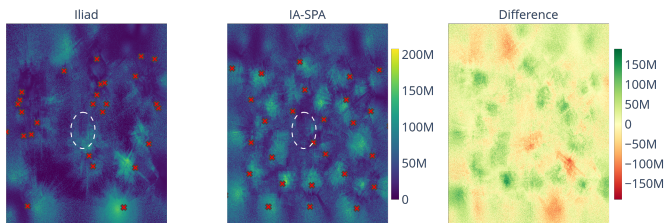


Fig. 11. Data rate distribution in Florence. The columns represent the Iliad baseline (left), IA-SPA optimization (center), and absolute gain (right). The dashed white ellipse indicates the exclusionary zone where transmitter placement is prohibited.

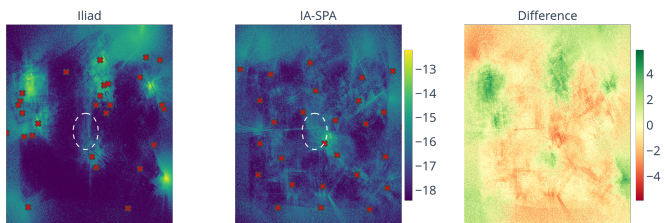


Fig. 12. Interference distribution in Florence. The columns represent the Iliad baseline (left), IA-SPA optimization (center), and absolute difference (right). The dashed white ellipse indicates the exclusionary zone where transmitter placement is prohibited.

A visual analysis of the heatmaps in Fig. 11 reveals how the algorithm compensates for the placement restriction. The IA-SPA strategically positions transmitters to exploit the urban geometry. The interference results in Fig. 12 further underscore the power of this site-specific approach. Despite the added complexity of the constraint, the IA-SPA delivers a 30% reduction in mean interference and a 50% reduction in peak interference relative to the Iliad deployment.

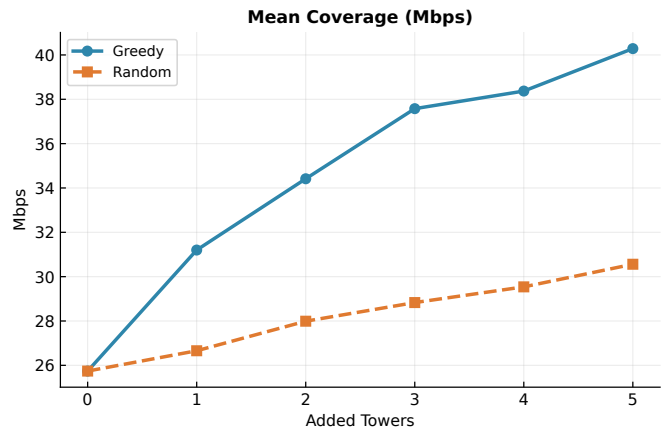


Fig. 13. Average data rate achieved by IA-SPA compared to the mean performance over 10 trials of random transmitter placement. The x-axis indicates the number of additional towers placed on top of the 9 existing AT&T towers in San Francisco, and the y-axis shows the resulting data rate.

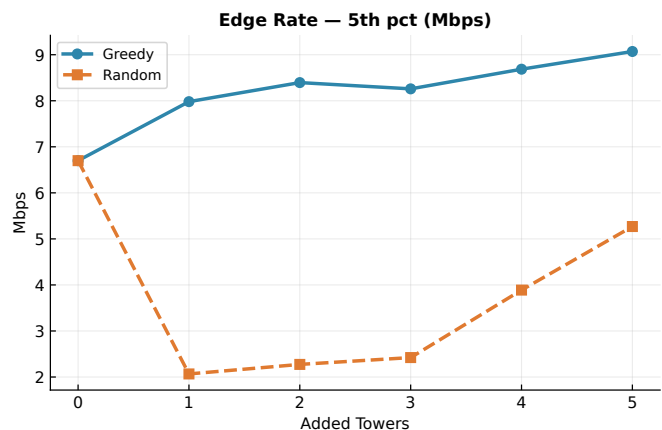


Fig. 14. Edge rate (5th percentile) comparison between IA-SPA and the mean performance over 10 trials of random placement. The x-axis indicates the number of additional towers placed on top of the 9 existing AT&T towers in San Francisco, and the y-axis shows the achieved data rate.

F. San Francisco with fixed Initial Deployment

In practice, transmitters are rarely deployed in empty environments without existing infrastructure. Instead, operators typically face a *continuous deployment* setting, where new transmitters must be placed to augment an existing network. To evaluate IA-SPA in this more realistic scenario, we initialize the system with the 9 transmitter locations deployed in San Francisco by AT&T (shown in Fig. 6). Starting from this baseline, IA-SPA sequentially determines up to 5 additional transmitter locations to improve network coverage. We assess performance by comparing against random transmitter placement, reporting results averaged over 10 independent trials to reduce variability due to randomness.

Figure 13 shows the average data rate as a function of the number of added transmitters. The blue curve corresponds to IA-SPA, while the orange curve shows the mean performance of 10 independent random placements. Even with the addition of a single transmitter, IA-SPA yields a substantial improvement over random placement.

Figure 14 presents the same comparison for the edge rate (5th percentile). IA-SPA again consistently outperforms random placement, with significant gains observed even when only a single transmitter is added.

TABLE V
PERFORMANCE METRICS: GREEDY VS. RANDOM PLACEMENT (+5
ADDED TOWERS, SAN FRANCISCO)

Metric	Random	IA-SPA	Change
<i>Data Rate [Mbps]</i>			
Mean Data Rate	30.56	40.29	↑+31.82%
Std. Dev.	23.09	31.46	↑+36.24%
Maximum Data Rate	156.56	176.17	↑+12.52%
Edge Rate (5%-tile)	5.27	9.07	↑+72.16%
<i>Interference [nW]</i>			
Mean Interference	8.93	7.92	↓-11.29%
Std. Dev.	28.01	20.71	↓-26.04%
Maximum Interference	1039.93	514.07	↓-50.57%

Table V provides a detailed comparison for the case where 5 additional transmitters are deployed. IA-SPA improves the average data rate by approximately 30% relative to random placement (averaged over 10 trials), while the edge rate increases by 72%. Additionally, IA-SPA reduces interference, achieving an 11% decrease in mean interference compared to random placement. This illustrates that IA-SPA is capable of yielding promising performance in realistic continuous deployment scenarios.

G. Key Takeaways from Results

The most significant results are found in the San Francisco AT&T scenario. Unlike other baselines that exhibit massive coverage gaps, the AT&T deployment is dense and well-structured. Despite this high-quality starting point, the IA-SPA achieved a 70% increase in mean throughput and a 88% improvement in the edge (5th percentile) data rate. These gains are particularly convincing because they were achieved while simultaneously slightly reducing the interference (by 2%). This proves that the algorithm is performing a high-precision optimization that disentangles overlapping signal footprints by exploiting the site-specific 3D geometry of the city.

The comparison between the two accumulation models highlights the distinction between raw signal capacity and interference-limited performance. While the \mathcal{P}_{SUM} configuration provides an idealized upper bound for throughput by assuming perfect coordination, it lacks the implicit pressure to avoid overlapping coverage areas. This is reflected in the numerical results. While IA-SPA still achieves significant gains when using \mathcal{P}_{SUM} , the improvements are noticeably lower than those seen under \mathcal{P}_{MAX} (e.g. 43% mean rate increase vs 70% for AT&T). This discrepancy suggests that by optimizing for aggregate power rather than strongest serving link, the algorithm may place transmitters in locations that provide redundant coverage, rather than expanding the network’s effective footprint. Consequently, the \mathcal{P}_{MAX} objective not only provides a more realistic representation of signal behavior, but also serves as a more effective driver for identifying strategic sites that mitigate the specific geometric “dead zone” characteristic for dense urban topologies.

The exclusionary zone and continuous deployment studies serve to demonstrate that the results of IA-SPA remain robust under various operational constraints. When considering an exclusionary zone, the algorithm achieved an 55% edge-rate improvement under placement constraints. Similarly we also showed that the algorithm is capable of incremental deployment by computing optimal transmitters to be added to an existing infrastructure, which resulted in a 29% improvement in data rate and a 30% reduction in interference.

V. CONCLUSION

In this paper, we introduced the Interference-Aware Submodular Placement Algorithm (IA-SPA), a framework that bridges the gap between theoretical submodular optimization and high-fidelity wireless physics. By integrating ray-tracing propagation data into an aggregated network quality functional $S(T)$, we moved beyond simplified geometric heuristics to a model that accounts for the complex interplay of 3D urban geometry, material properties, and signal interference.

We provide a theoretical optimality guarantee relative to the global optimum and our numerical evaluations demonstrate that the IA-SPA provides substantial performance elevations across all tested scenarios. Most notably, the algorithm proved its ability to significantly enhance even high-quality deployments, such as the AT&T baseline in San Francisco, by optimizing for both mean throughput and edge-user reliability while lowering the interference floor. Furthermore, we showed that the framework is highly adaptable to modern deployment challenges, including geographical exclusionary zones and incremental network densification. These results suggest that as wireless networks move toward the higher-frequency, geometry-sensitive regimes of 5G-Advanced and 6G, the shift from stochastic planning to site-specific, submodular optimization will be essential for realizing true network potential.

Several promising directions for future work remain. First, while our algorithm currently assumes uniform tower costs, extending the framework to handle heterogeneous costs would allow for the joint optimization of location and power usage, or the deployment of mixed base station types (e.g., macro vs. small cells). Second, while the utility function \bar{W} effectively balances coverage and interference, the optimal choice of its parameters remains open. Exploring machine learning approaches to tune these parameters for specific urban topologies could further improve performance. Finally, integrating reinforcement learning could evolve the current strategy into a more global scheme, utilizing changes in $S(T)$ as a reward signal to overcome the inherent sequential approach.

REFERENCES

- [1] J. G. Andrews, T. Humphreys, and T. Ji, “6G takes shape,” *IEEE BITS the Information Theory Magazine*, 2025.
- [2] O. Yildiz, “Digital twin-based ray tracing analysis for antenna orientation optimization in wireless networks,” *Electronics*, vol. 14, no. 15, p. 3023, 2025.
- [3] S. Jiang, Q. Qu, X. Pan, A. K. Agrawal, R. Newcombe, and A. Alkhatieb, “Learnable wireless digital twins: Reconstructing electromagnetic field with neural representations,” *IEEE Open Journal of the Communications Society*, vol. 6, pp. 1568–1590, 2025.
- [4] J. O’Rourke, *Art Gallery Theorems and Algorithms*. Oxford, UK: Oxford University Press, 1987.

- [5] I. Bjorling-Sachs and D. L. Souvaine, "An efficient algorithm for guard placement in polygons with holes," *Discrete & Computational Geometry*, vol. 13, pp. 77–109, 1995. [Online]. Available: <https://api.semanticscholar.org/CorpusID:37188717>
- [6] S. K. Ghosh, J. W. Burdick, A. Bhattacharya, and S. Sarkar, "Online algorithms with discrete visibility - exploring unknown polygonal environments," *IEEE Robotics & Automation Magazine*, vol. 15, no. 2, pp. 67–76, 2008.
- [7] Y. Cho, J. Won, D.-Y. Kim, and J.-W. Lee, "Optimal placement of aerial base station utilizing topographic features," *IEEE Internet of Things Journal*, vol. 12, no. 12, p. 19882, 2025.
- [8] D. T. Lee and F. P. Preparata, *Computational Geometry: A Survey*. IEEE Computer Society Press, 1986, reprinted in *IEEE Transactions on Computers*, vol. C-33, no. 12, pp. 1072–1101, 1984.
- [9] A. Krause and D. Golovin, "Submodular function maximization," in *Tractability: Practical Approaches to Hard Problems*. Cambridge University Press, 2011, pp. 71–104.
- [10] E. Amaldi, A. Capone, and F. Malucelli, "Planning UMTS base station location: Optimization models with power control and algorithms," *IEEE Transactions on Wireless Communications*, vol. 2, no. 5, pp. 939–952, 2003.
- [11] A. Bircher, M. Kamel, K. Alexis, H. Oleynikova, and R. Siegwart, "Receding horizon path planning for 3D exploration and surface inspection," *Autonomous Robots*, vol. 42, pp. 291–306, 2018.
- [12] H. H. Gonzalez-Baños and J.-C. Latombe, "Navigation strategies for exploring indoor environments," in *Intl. Symposium on Experimental Robotics (ISER)*. Springer, 2002, pp. 749–758.
- [13] L. Ly and Y.-H. R. Tsai, "Autonomous exploration, reconstruction, and surveillance of 3d environments aided by deep learning," in *2019 International Conference on Robotics and Automation (ICRA)*, 2019, pp. 5467–5473.
- [14] M. Popovic, F. Thomas, S. Papatheodorou, N. Funk, T. Vidal-Calleja, and S. Leutenegger, "Volumetric occupancy mapping with probabilistic depth completion for robotic navigation," *IEEE Robotics and Automation Letters*, vol. 6, pp. 5072–5079, 2021.
- [15] L. Taus and Y.-H. R. Tsai, "Optimizing sensor network design for multiple coverage," arXiv preprint arXiv:2309.08545, 2024.
- [16] J. Hoydis, S. Cammerer, F. A. Aoudia, A. Vem, N. Binder, G. Marcus, and A. Keller, "Sionna: An open-source library for next-generation physical layer research," arXiv preprint arXiv:2203.11854, 2022.
- [17] M. G. Aram, H. Guo, M. Yin, and T. Svensson, "Site-specific outdoor propagation assessment and ray-tracing analysis for wireless digital twins," 2024. [Online]. Available: <https://arxiv.org/abs/2410.14620>
- [18] A. Uwaechia and N. Mahyuddin, "A comprehensive survey on millimeter wave communications for fifth-generation wireless networks: Feasibility and challenges," *IEEE Access*, vol. 8, pp. 62 367–62 414, 2020.
- [19] M. D. Renzo, A. Zappone, M. Debbah, M.-S. Alouini, C. Yuen, J. de Rosny, and S. Tretjakov, "Smart radio environments empowered by reconfigurable intelligent surfaces: How it works, state of research, and road ahead," *IEEE Journal on Selected Areas in Communications*, 2020.
- [20] X. Gao, W. Yi, A. Agapitos, H. Wang, and Y. Liu, "Coverage and capacity optimization in STAR-RISs assisted networks: A machine learning approach," in *IEEE Wireless Communications and Networking Conference (WCNC)*, 2023, pp. 1–6.
- [21] S. Beyraghi, J. Shabanpour, G. Geraci, P. Almasan, and A. Lozano, "Data-driven deployment of reconfigurable intelligent surfaces in cellular networks," *IEEE Journal on Selected Areas in Communications*, vol. 44, pp. 2938–2951, 2026.
- [22] M. Belgiovine, C. Dick, and K. Chowdhury, "Better together: Leveraging multiple digital twins for deployment optimization of airborne base stations," *IEEE Transactions on Mobile Computing*, vol. 25, no. 3, pp. 3920–3935, 2026.
- [23] L. Qian, Y. J. Zhang, and J. Huang, "MAPEL: Achieving global optimality for a non-convex wireless power control problem," 2008. [Online]. Available: <https://arxiv.org/abs/0805.2675>
- [24] M. Chiang, C. W. Tan, D. P. Palomar, D. O'Neill, and D. Julian, "Power control by geometric programming," *IEEE Transactions on Wireless Communications*, vol. 6, no. 7, pp. 2640–2651, 2007.
- [25] J. Huang, R. Berry, and M. Honig, "Distributed interference compensation for wireless networks," *IEEE Journal on Selected Areas in Communications*, vol. 24, no. 5, pp. 1074–1084, 2006.
- [26] D. Julian, M. Chiang, D. O'Neill, and S. Boyd, "QoS and fairness constrained convex optimization of resource allocation for wireless cellular and ad hoc networks," in *IEEE INFOCOM*, vol. 2, 2002, pp. 477–486.
- [27] P. Hande, S. Rangan, M. Chiang, and X. Wu, "Distributed uplink power control for optimal SIR assignment in cellular data networks," *IEEE/ACM Transactions on Networking*, vol. 16, no. 6, pp. 1420–1433, 2008.
- [28] M. Chen, S. L. Herbert, H. Hu, Y. Pu, J. F. Fisac, S. Bansal, S. Han, and C. J. Tomlin, "FaSTrack: A modular framework for real-time motion planning and guaranteed safe tracking," *IEEE Transactions on Automatic Control*, vol. 66, no. 12, pp. 5861–5876, 2021.
- [29] F. Khoramnejad and E. Hossain, "Generative AI for the optimization of next-generation wireless networks: Basics, state-of-the-art, and open challenges," 2024. [Online]. Available: <https://arxiv.org/abs/2405.17454>
- [30] A. Pasqual, S. Edirisinghe, C. A. Chan, and A. Nirmalathas, "Optimized base station deployment and assignment for smart factory millimeter wave networks," in *IEEE Annual Conference of the Industrial Electronics Society (IECON)*. IEEE, 2024.
- [31] J. Qiu, J. Lyu, and L. Fu, "Placement optimization of aerial base stations with deep reinforcement learning," in *IEEE International Conference on Communications (ICC)*, 2020, pp. 1–6.
- [32] B. Omoniwa, B. Galkin, and I. Dusparic, "Energy-aware optimization of UAV base stations placement via decentralized multi-agent Q-learning," in *IEEE Consumer Communications & Networking Conference (CCNC)*, 2022, pp. 216–222.
- [33] M. Umer, M. A. Mohsin, A. Kaushik, Q.-U.-A. Nadeem, A. A. Nasir, and S. A. Hassan, "Reconfigurable intelligent surface-assisted aerial nonterrestrial networks: An intelligent synergy with deep reinforcement learning," *IEEE Vehicular Technology Magazine*, vol. 20, no. 1, pp. 55–64, 2025.
- [34] K. Sato and K. Suto, "Bayesian optimization framework for channel simulation-based base station placement and transmission power design," *IEEE Networking Letters*, vol. 6, no. 4, pp. 217–221, 2024.
- [35] E. Nwelih, J. Isabona, and A. L. Imoize, "Optimization of base station placement in 4G LTE broadband networks using adaptive variable length genetic algorithm," *SN Comput. Sci.*, vol. 4, no. 2, Dec. 2022. [Online]. Available: <https://doi.org/10.1007/s42979-022-01533-y>
- [36] F. Erden, C. K. Anjinappa, E. Ozturk, and I. Guvenc, "Outdoor mmWave base station placement: A multi-armed bandit learning approach," 2020. [Online]. Available: <https://arxiv.org/abs/2003.03494>
- [37] S. Das and A. Chakraborty, "SKYSCALE: A radio tomographic approach towards scaling UAV network deployments," in *ACM Intl. Symposium on Mobile Ad Hoc Networking and Computing (MobiHoc)*. ACM, 2024.
- [38] D. Romero, P. Q. Viet, and G. Leus, "Aerial base station placement leveraging radio tomographic maps," in *IEEE Intl. Conference on Acoustics, Speech and Signal Processing (ICASSP)*, 2022, pp. 5358–5362.
- [39] D. Romero, P. Q. Viet, and R. Shrestha, "Aerial base station placement via propagation radio maps," *IEEE Transactions on Communications*, vol. 72, no. 9, pp. 5349–5364, 2024.
- [40] Y. Wang, J. Lyu, and L. Fu, "Fast online movement optimization of aerial base stations based on global connectivity map," in *IEEE Vehicular Technology Conference (VTC2025-Fall)*, 2025, pp. 1–6.
- [41] J. Lyu, X. Chen, J. Zhang, and L. Fu, "Spatial deep learning for site-specific movement optimization of aerial base stations," *IEEE Transactions on Wireless Communications*, vol. 23, no. 7, pp. 7712–7727, 2024.
- [42] E. Tekgul, T. Novlan, S. Akoum, and J. G. Andrews, "Joint uplink-downlink capacity and coverage optimization via site-specific learning of antenna settings," *IEEE Transactions on Wireless Communications*, vol. 23, no. 5, pp. 4032–4048, 2024.
- [43] M. Mallik and G. Villemaud, "Base station deployment under EMF constraints by deep reinforcement learning," 2025. [Online]. Available: <https://arxiv.org/abs/2601.02385>
- [44] T. Shi, W. Wen, P. Wu, and M. Xia, "Vertical heterogeneous networks beyond 5G: CoMP coverage enhancement and optimization," *IEEE Transactions on Wireless Communications*, vol. 25, pp. 9391–9405, 2026.
- [45] City and County of San Francisco, "Existing Commercial Wireless Telecommunication Service Facilities," SF Open Data, 2025, available: https://data.sfgov.org/Geographic-Locations-and-Boundaries/Existing-Commercial-Wireless-Telecommunication-Ser/aa26-h926/about_data.
- [46] Unwired Labs, "OpenCellID: The world's largest open database of cell towers," <https://opencellid.org/>, 2026, accessed: Jan 14, 2026.